



HAL
open science

Complex Urban Atmospheres alters Alveolar Stem Cells Niche Properties and drives Lung Fibrosis Running: Urban atmosphere disrupts alveolar stem cell niche One-sentence summaries: Complex Urban Atmospheres alter Alveolar Stem Cell Niche Properties and induces Lung Fibrosis

Randa Belgacemi, Bruno Ribeiro Baptista, Grégoire Justeau, Marylène Toigo, Andrew Frauenpreis, Rojda Yilmaz, Audrey Der Vartanian, Mathieu Cazaunau, Edouard Pangui, Antonin Bergé, et al.

► **To cite this version:**

Randa Belgacemi, Bruno Ribeiro Baptista, Grégoire Justeau, Marylène Toigo, Andrew Frauenpreis, et al.. Complex Urban Atmospheres alters Alveolar Stem Cells Niche Properties and drives Lung Fibrosis Running: Urban atmosphere disrupts alveolar stem cell niche One-sentence summaries: Complex Urban Atmospheres alter Alveolar Stem Cell Niche Properties and induces Lung Fibrosis. American Journal of Physiology - Lung Cellular and Molecular Physiology, 2023, 325 (4), pp.L447-L459. 10.1152/ajplung.00061.2023 . inserm-04617326

HAL Id: inserm-04617326

<https://inserm.hal.science/inserm-04617326>

Submitted on 19 Jun 2024

HAL is a multi-disciplinary open access archive for the deposit and dissemination of scientific research documents, whether they are published or not. The documents may come from teaching and research institutions in France or abroad, or from public or private research centers.

L'archive ouverte pluridisciplinaire **HAL**, est destinée au dépôt et à la diffusion de documents scientifiques de niveau recherche, publiés ou non, émanant des établissements d'enseignement et de recherche français ou étrangers, des laboratoires publics ou privés.

1 **Complex Urban Atmospheres alters Alveolar Stem Cells Niche Properties**
2 **and drives Lung Fibrosis**

3
4 **Running:** Urban atmosphere disrupts alveolar stem cell niche

5
6 **One-sentence summaries:** Complex Urban Atmospheres alter Alveolar Stem Cell Niche
7 Properties and induces Lung Fibrosis.

8
9 Randa Belgacemi^{1,2}, Bruno Ribeiro Baptista¹, Grégoire Justeau¹, Marylène Toigo¹, Andrew
10 Frauenpreis², Rojda Yilmaz¹, Audrey Der Vartanian¹, Mathieu Cazaunau⁴, Edouard Pangui⁴,
11 Antonin Bergé⁵, Aline Gratien⁵, Juan Camilo Macias Rodriguez⁵, Saverio Bellusci³,
12 Geneviève Derumeaux¹, Jorge Boczkowski¹, Denise Al Alam², Patrice Coll⁵, Sophie Lanone¹,
13 Laurent Boyer^{1,5}
14

15 1. Univ Paris Est Créteil, INSERM, IMRB, FHU Senec, F-94010, Créteil, France

16 2. Lundquist Institute for Biomedical Innovation, Harbor-UCLA Medical Center,
17 Torrance, California, USA

18 3. German Center for Lung Research (DZL), Department of Pulmonary and Critical
19 Care Medicine and Infectious Diseases, Cardio-Pulmonary Institute (CPI),
20 Universities of Giessen and Marburg Lung Center (UGMLC), Justus Liebig
21 University Giessen, Giessen, Germany

22 4. Univ Paris Est Créteil and Université Paris Cité, CNRS, LISA, F-94010, Créteil,
23 France

24 5. Université Paris Cité and Univ Paris Est Créteil, CNRS, LISA, F-75013, Paris,
25 France.

26
27
28 To whom correspondence should be addressed:

29
30 Laurent Boyer, E-mail : Laurent.boyer@aphp.fr
31 [Randa Belgacemi, E-mail : randa.belgacemi@lundquist.org](mailto:Randa.Belgacemi@lundquist.org)
32

33 **Abstract**

34

35 **Introduction:** There is growing evidence suggesting that urban pollution has adverse effects
36 on lung health. However, how urban pollution affects alveolar mesenchymal and epithelial
37 stem cell niches remains unknown.

38

39 **Aim:** Determine how complex representative urban atmospheres alter alveolar stem cell niche
40 properties.

41

42 **Methods:** Mice were placed in an innovative chamber realistically simulating the atmosphere
43 of a megalopolis, or “clean air”, for 7 days. Lungs were collected and fibroblasts and
44 epithelial cells (EpCAM⁺) were isolated. Fibroblasts proliferative capacities were tested by
45 population doubling levels (PDL) and microarray analyses were performed. Fibroblasts and
46 EpCAM⁺ cells from exposed, non-exposed or naive mice were co-cultured in organoid assays
47 to assess the stem cell properties. Collagen deposition (Sirius red), lipofibroblasts (ADRP,
48 COL1A1), myofibroblasts (α SMA), alveolar type 2 cells (AT2, SFTPC⁺) and alveolar
49 differentiation intermediate cell (ADI, KRT8⁺/CLDN4⁺) markers were quantified in the
50 lungs.

51

52 **Results:** Fibroblasts obtained from mice exposed to urban atmosphere had lower PDL and
53 survival and produced fewer and smaller organoids. Microarray analysis showed a decrease of
54 adipogenesis, and an increase of genes associated with fibrosis suggesting a lipofibroblast to
55 myofibroblast transition. Collagen deposition and myofibroblast number increased in the lung
56 of urban atmosphere exposed mice. AT2 number was reduced and associated with an increase
57 of ADI cells KRT8⁺/CLDN4⁺. Furthermore, EpCAM⁺ cells from exposed mice also produced
58 fewer and smaller organoids.

59

60 **Conclusions:** Urban atmosphere alters alveolar mesenchymal stem cell niche properties by
61 inducing a lipofibroblast to myofibroblast shift. It also results in alveolar epithelial
62 dysfunction and a fibrotic-like phenotype.

63

64 Key words: Urban, Complex atmosphere, alveolar stem cell niche, lung

65

66

67

68 **New & Noteworthy**

69 Urban pollution is known to have major adverse effects on lung health. To assess the effect of
70 pollution on alveolar regeneration, we exposed adult mice to a simulated high pollution urban
71 atmosphere, using an innovative CESAM simulation chamber (<https://cesam.cnrs.fr/>). We
72 demonstrated that urban atmosphere alters alveolar mesenchymal stem cell niche properties
73 by inducing a lipofibroblast to myofibroblast shift and induces alveolar epithelial dysfunction.

74

75

76 **Introduction**

77 A report by the European Environment Agency estimates that in Europe, nearly 95% of the
78 urban population is exposed to concentrations of fine particles exceeding WHO guidelines ¹.

79 The nature of the particles in urban air is very heterogeneous and composed of thousands of
80 micro-pollutants, in the gaseous or particulate phase; combustion aerosols (soot), inorganic
81 aerosols (e.g., agricultural origin), secondary organic aerosols (e.g., produced by urban and
82 peri-urban chemistry) and aerosols of terrigenous origin (e.g., erosion), from PM1 (ultrafine)
83 to PM10 (coarser particles) ²⁻⁴. These components generate several hundred thousand
84 chemical reactions, particularly under the impact of solar energy ⁵⁻⁷. Based on
85 epidemiological data, there is a growing body of evidence linking exposure to urban air
86 pollution to lung function alterations and the development of adult respiratory diseases,
87 particularly chronic bronchial diseases ⁸⁻¹⁰. A causal link with the urban pollution exposure is
88 suggested in interstitial lung diseases but remains controversial, particularly because
89 epidemiological studies are limited in size and did not consider a multipollutant exposure
90 model ¹¹⁻¹³. Thus, how epithelial alveolar stem cells and their environment are affected by air
91 pollution and how this process induces lung pathology is yet to be determined ¹⁹⁻²¹.

92 Alveolar epithelial type 2 (AT2) cells represent the predominant alveolar epithelial progenitor
93 cells ¹⁴. They proliferate and differentiate into alveolar epithelial type 1 (AT1) cells through
94 intermediate states ^{15,16}. The AT2 behavior is influenced by paracrine signals from its
95 surrounding environment (niche) such as the mesenchyme ¹⁷⁻¹⁹. Depending on its
96 characteristics, the mesenchymal alveolar niche can either support alveolar growth and
97 regeneration or induce deleterious effects ^{20,21}. The lung resident mesenchymal cells that
98 compose the niche are more functionally classified by their abilities (niche properties) to
99 support epithelial cell growth. Among them, lipofibroblasts, lipid-droplet-containing
100 interstitial fibroblasts that have many similarities with adipocytes, are an important
101 subpopulation with niche properties ^{22,23}. In interstitial lung diseases, such as idiopathic
102 pulmonary fibrosis, they lose their niche characteristics by differentiating to myofibroblasts,
103 thus promoting fibrosis ^{24,25}.

104 Therefore, we hypothesized that urban megalopolis pollution, such as Beijing atmosphere,
105 alters both the alveolar mesenchymal and epithelial stem cell properties leading to a fibrosis-
106 like phenotype. To overcome the limitations of solely exposing organisms to isolated
107 components of air pollution and disregarding the potential synergistic effects among its
108 constituents, we used a multi-component pollutant exposure atmospheric simulation chamber.

109 We have combined this modern approach with the use of organoid culture ^{26,27}, in order to
110 assess the stem cell niche capacities ²⁸⁻³⁰.

111

112

113

114

115

116

117

118

119

120

121

122

123

124

125

126

127

128

129

130

131

132

133

134

135

136

137 **METHODS**

138 **Ethics statements**

139 The French Institutional Animal Care and Use Committee approved experimental procedures
140 on mice (APAFIS#30121-2021022511414629 v9). Animal experiments were carried out in
141 compliance with the guidelines and regulations of the Institut national de la santé et de la
142 recherche médicale (Inserm).

143

144 **Animal models**

145 Animal use was approved by the French Institutional Animal Care Committee. Equal numbers
146 of male and female mice were used. C57BL/6JRj mice were housed in a pathogen-free barrier
147 environment throughout the study (12 h light/dark cycle with access to food and water ad
148 libitum).

149

150 **Generation and characterization of urban complex atmosphere**

151 The generation and characterization of the urban complex atmosphere and the exposure of
152 mice were performed by LISA (UMR CNRS 7583, Créteil, France). The Laboratoire
153 Interuniversitaire des Systèmes Atmosphériques (LISA), in Créteil, has developed an
154 atmospheric simulation chamber (www.cesam.cnrs.fr). The experimental set-up allows the
155 continuous injection, in the exposure chamber, of mixtures of primary pollutants (NO_x,
156 organic compounds representative of anthropogenic emissions, SO₂, soot, mineral dusts) at
157 low concentration (ppb). The residence time of the air thus formed in the chamber is a few
158 hours, calculated to represent the air masses on a regional scale. During this time, the
159 synthetic mixture is exposed to solar radiation, allowing the formation of secondary pollutants
160 such as ozone, NO, formaldehyde. Each of these parameters (nature of the initially injected
161 pollutants, methods of "aging" of the atmospheres, etc) can be modulated according to the
162 characteristics of the desired model atmosphere. The CESAM experimental chamber is
163 equipped with numerous analytical instruments and benefits from the LISA's dedicated
164 atmospheric chemistry instrumentation: analysis of gaseous pollutants (ozone, NO, NO₂, SO₂,
165 CO, CO₂, VOC in particular), and of aerosol properties (particle size and mass distributions,
166 hygroscopy, etc) - see <http://www.cesam.cnrs.fr/index.php?p=2> for more information. LISA
167 atmospheric chambers simulated a highly polluted urban area with a level of pollution: this
168 mixture aimed at reproducing the air of megacities such as Beijing, in condition of pollution

169 alert as it is more and more frequently the case. The primary sources of pollutants here
170 include diesel emissions coal combustion, sandstorms from the north, and dust from local
171 construction. The pollutants content was measured and validated as described in details by
172 Guilloteau et al., 2022.³¹. A control experimental group was exposed to unpolluted air (i.e.,
173 atmosphere from the room, filtered *via* a HEPA filter to remove particles and b) denuders to
174 remove reactive trace species: O₃, NO_x, VOCs, etc.).

175

176 **Histological analysis**

177 Murine lungs were fixed in 4% paraformaldehyde, embedded in paraffin, and sectioned at
178 5µm thickness. Sirius Red staining was performed according to standard procedures and
179 slides were pictured at 20X magnification using Axioimager M2 (Zeiss, GE). Positive red
180 Sirius areas excluded large airways and vessels were quantified on 10 random pictures per
181 slides by using Halo area quantification module.

182 **Immunofluorescence**

183 Mice lung sections were stained as standard protocol. Briefly, slides were rehydrated and
184 boiled in a citrate antigen retrieval solution for 20 minutes (min). If needed, a
185 permeabilization step with 0.2% Saponin for 10 min was performed. Tissues were saturated
186 using 3% BSA in PBS for 30 min. Sections were incubated overnight with primary antibodies
187 at 4°C and, then stained with appropriate fluorochrome-conjugated secondary antibodies
188 when necessary. Nuclei were counterstained with DAPI (DE571; Life Technologies, Grand
189 Island, NY, USA) and mounted using ProLong Diamond Antifade Mounting (Life
190 Technologies). Antibodies are detailed in Table 1. Image acquisition was performed using
191 fluorescence microscope (Axioimager M2, Zeiss). Ten random pictures were taken from each
192 slide and the quantification of the different staining was performed using the HALO® Image
193 Analysis Platform version 3.4.2986 Highplex FL module (Indica Labs, Inc; Albuquerque,
194 NM). The staining quantification by Halo excluded large airways and vessels by using the
195 classifier module.

196

197

198

199

200

201 **Table 1:** Primary Antibodies used in immunofluorescence

Antibody	Company	Catalogue number	RRID	Host species	Dilution
Vimentin	Abcam, Cambridge, UK	Ab92547	AB_10562134	Rabbit	1:200
Pan-cytokeratin	Abcam, Cambridge, UK	Ab6401	AB_305450	Mouse	1:200
CD31	Abcam, Cambridge, UK	Ab124432	AB_2802125	Rabbit	1:200
ADRP/PLIN2	Proteintech, Rosemont, IL, USA	15294-1-AP	AB_2878122	Rabbit	1:100
α SMA-Cy3 Conjugated	Sigma-Aldrich St. Louis, MO, USA	C6198	AB_476856	Mouse	1:200
SFTPC	Abcam, Cambridge, UK	Ab90716	AB_10674024	Rabbit	1:200
KI67- eFluor™ 570	eBioscience, Waltham, MA, USA	41-5698-80	AB_11219874	Rat	1:300
KRT8	DSHB, Iowa City, IA, USA	TROMA-I	AB_531826	Rat	1:250
Claudin-4	Proteintech, Rosemont, IL, USA	16165-1-AP	AB_2279763	Rabbit	1:100

202

203 **Isolation and culture of murine fibroblasts**

204 Primary lung fibroblasts were isolated from mice lungs, exposed or not to urban pollution,
 205 after enzymatic and mechanic dissociation. In brief, lung was perfused with ice-cold D-PBS
 206 supplemented with 1% antibiotic-antimycotic (anti-anti, Gibco, MA, USA) through the right
 207 ventricle, excised and minced in small homogeneous pieces in dispase (50 U/ml, Corning,

208 NY, USA), type 1 collagenase (310 U/mg, Life Technologies, CA, USA), DNase 1 (154,2
209 UI/ μ L) and placed in a GentleMACS Octodissociator (Miltenyi, GE) for 45 min at 37°C. After
210 digestion, the solution was filtered into 70- and 40- μ m strainer (Corning), washed and plated
211 in Dulbecco's Modified Eagle's Medium/F12 (DMEM/F12, Invitrogen, CA, USA)
212 supplemented with 1% anti-anti (Gibco) and 10% FBS (Eurobio, FR). Six hours post plating,
213 supernatant with non-adhesive cells were removed and replaced. Purity of culture was
214 assessed by staining for positive vimentin and absence of staining for α SMA, CD31 and pan-
215 cytokeratin (See Table 3). Cells were passage using 0,05% trypsin-EDTA (Gibco) and the
216 cumulative population doubling level (PDL) was recorded.

217 **Isolation of murine epithelial cells**

218 Murine epithelial cells (EpCAM+) were obtained following enzymatic and mechanical
219 digestion of the lung tissue as described above. Cells obtained were subjected to a negative
220 magnetic bead sort to exclude endothelial and immune (Ter119-CD31-CD45-LNGFR-
221 CD16/32-CD90; Miltenyi) followed by a positive magnetic bead sorting for the epithelial
222 marker CD326+(Miltenyi) using LS Columns (Miltenyi; See Table 3).

223

224 **Microarray analyses**

225 Total RNA was extracted using the RNeasy Protect Mini Kit (Quiagen, GE), according to the
226 manufacturer's instructions, and quantified using a NanoDrop 2000c (Thermo Scientific,
227 USA). RNA quality was assessed using the TapeStation 4150 (Agilent, USA). All samples
228 passed quality control standards of minimum concentration and RNA Quality Indicator
229 (RQN) >9, with discrete 18S and 28S bands. cDNA libraries were generated from 1000 ng of
230 total RNA using the Illumina Stranded Total RNA prep, Ligation with Ribo-Zero Plus
231 (Illumina, USA) following the manufacturer's instructions. Sequencing was performed on the
232 NextSeq 500 sequencing system (Illumina). Quality assessment of raw sequences and
233 trimming were performed by trimmomatic (version 0.39). Significant DEGs were inputted
234 into ToppFun to find differentially regulated pathways and disease phenotypes³². Only
235 pathways that were significant after being adjusted for FDR were reported. R (version 4.1.2)
236 and RStudio (version 2022.07.0+358) were used to create the volcano plot of DEGs (Fig 3A),
237 the bar graph of significant pathways (Fig 3B), and the heat map of DEGs for fibrosis and
238 adipogenesis (Fig 3C). The packages tidyverse (version 1.3.2) and ggsci (version 2.9) were
239 used for plot construction.

240 **Alveolar organoids**

241 At the 2nd passage, 50000 fibroblasts were cocultured with 20 000 EpCAM+. Cells were
242 resuspended in SABM (Lonza, CH) and mix with matrigel (Corning) at a ratio of 1/1 and
243 added to a 24-well transwell filter inserts with 0.4 microns pore (Corning) in a 24 well tissue
244 culture plate containing 500µL of medium (SABM). The medium was supplemented with
245 ROCK inhibitor (Sigma Aldrich, MO, USA) for the first 48 hours than changed every 2 days.
246 Cultures were incubated at 37°C in a humidified incubator (5% CO₂). After 14 and 21 days of
247 growth, obtained lung organoids were pictured (x10, Axioimager M2, Zeiss), counted, and
248 measured with ImageJ.

249 **Real-time PCR analyses**

250 RNA was extracted using the RNeasy Protect Mini Kit (Quiagen). RNA was reverse
251 transcribed into cDNA using the High-Capacity cDNA Reverse Transcription Kit (Applied
252 Biosystems, MA, USA) according to the manufacturer's instructions. PCR products were
253 amplified using specific TaqMan gene expression assays (listed in Table 2, Applied
254 Biosystems) and the TaqMan Universal PCR Master Mix II (Applied Biosystems). PCR
255 products were detected using the Quantstudio 6 (Applied Biosystems). Each sample was run
256 in triplicate.

257 **Table 2:** TaqmanTM probes used for RT-qPCR

Target Gene	Probe ID
<i>ACTA2</i>	Mm00725412_s1
<i>FGF10</i>	Mm00433275_m1
<i>GAPDH</i>	Mm99999915_g1
<i>ADRP</i>	Mm00475794_m1
<i>COL1A1</i>	Mm00801666_g1
<i>WNT4</i>	Mm01194003_m1

258

259 **Statistical analyses**

260 Statistical analyzes were performed by the non-parametric Mann–Whitney and Kruskal–
261 Wallis tests. The results were considered significant if $p \leq 0.05$. Data were presented as mean
262 values \pm SEM. Analyzes were performed using GraphPad Prism 8.00 software (GraphPad
263 Prism Software Inc., CA, USA).

264 **TABLE 3: TABLE RESSOURCE**

REAGENT or RESOURCE	SOURCE	IDENTIFIER
Antibodies		
Biotin anti-Mouse TER-119/Erythroid Cell	Miltenyi	Cat# 130-112-907
Biotin anti-Mouse CD31	Miltenyi	Cat# 130-111-539
Biotin anti-Mouse CD45	Miltenyi	Cat# 130-110-795
Biotin anti-Mouse CD271 (LNGFR)	Miltenyi	Cat# 130-122-980
Biotin anti-Mouse CD16/32	Miltenyi	Cat# 130-107-038
Biotin anti-Mouse CD90	Miltenyi	Cat# 130-101-908
Anti-biotin microbeads	Miltenyi	Cat# 130-090-485
Anti-mouse CD326(EPCAM) microbeads	Miltenyi	Cat# 130-105-958
Anti-mouse IgM microbeads	Miltenyi	Cat# 130-047-302
FCR blocking	Miltenyi	Cat# 130-092-575
Anti-Vimentin	Abcam	Cat# ab92547; RRID:AB_10562134
Anti-Pan-cytokeratin	Abcam	Clone PCK-26; Cat# ab6401; RRID:AB_305450
Anti-CD31	Abcam	Cat# ab124432; RRID:AB_2802125
Anti-ADRP	Proteintech	Cat# 152941AP; RRID:AB_2878122
Anti- α SMA	Sigma Aldrich	Clone 1A4; Cat# C6198; RRID:AB_476856
Anti-SFTPC	Abcam	Cat# ab90716; RRID:AB_10674024
Anti-KI67	eBioscience	Cat# 41-5698-80; RRID:AB_11219874
Anti-KRT8	DSHB	Cat# TROMA-I; RRID:AB_531826
Anti-Claudin 4	Proteintech	Cat# 16165-1-AP; RRID:AB_2279763
Chemicals, peptides, and recombinant proteins		
DMEM/F12	Gibco	Cat# 21331020
SABM	Lonza	Cat# CC-3119
Anti-Anti	Gibco	Cat# 15240062
Growth factor reduced Matrigel	Corning	Cat# 356230
FBS	Eurobio	CVFSVF00
Dispase	Corning	Cat# 354235
Type I Collagenase	Life Technologies	Cat# 17100-017
ROCK inhibitor	Sigma Aldrich	Cat# Y0503
ACK lysis buffer	Invitrogen	Cat# 00-4333-57
DNase I	Sigma Aldrich	Cat# 10104159001
EDTA	Invitrogen	Cat# AM9912
0,25% Trypsin-EDTA	Gibco	Cat# 25200056
Applied Biosystems™ TaqMan™ Fast Advanced Master Mix	Applied Biosystems	Cat# 4444963
Mouse GAPDH Taqman probe Mm99999915_g1	Thermofisher	4453320
Mouse Acta2 Taqman probe Mm00725412_s1	Thermofisher	4453320
Mouse ADRP Taqman probe Mm00475794_m1	Thermofisher	4453320
Mouse COL1A1 Taqman probe Mm00801666_g1	Thermofisher	4453320

Mouse FGF10 Taqman probe Mm00433275_m1	Thermofisher	4453320
Critical commercial assays		
RNeasy Protect Mini Kit	Quiagen	Cat# QIA74126PK
High-Capacity cDNA Reverse Transcription Kit	Applied Biosystems™	Cat# 4368813
Deposited data		
Raw RNA-sequencing data of	This paper	GEO: <i>In progress</i>
Experimental models: Organisms/strains		
Mouse: C57BL/6JRj	Janvier Labs	Strain code: 000664
Software and algorithms		
ImageJ/Fiji	Schindelin et al., 2012	https://imagej.net/software/Fiji
Halo	Indicalab	https://indicalab.com/
Graphpad Prism 9	Dotmatics	www.graphpad.com
R	R Core Team, 2020	http://www.R-project.org/
Toppfun	Cincinnati Children's Hospital Medical Center	https://toppgene.cchmc.org/enrichment.jsp
Other		
0.4um Transwell Inserts (polyester)	Corning	Cat# 353095
ProLong™ Diamond Antifade Mountant	Molecular Probes	Cat# P36961
DAPI	Life Technologies	Cat# DE571
D-PBS	Gibco	Cat# 14190094

265
266
267

268
269
270
271
272
273
274
275
276

277 **Results**

278 **Atmospheric simulation chamber generates an urban atmosphere**

279 The atmospheric situation of a megalopolis like Beijing results from a complex equation,
280 initiated by traffic, industrial emissions, and the meteorological conditions. To better
281 understand the effect of the pollution on physiological processes we developed an innovative
282 platform modeling specific atmospheres in a small scale (Figure 1A and B)³³. Thus, to mimic
283 megalopolis urban atmosphere, as precursors, VOCs (Volatile Organic Compounds;
284 isopentane, propene, acetylene, acetaldehyde, benzene, toluene, and m,p-xylene), were first
285 introduced into the smog chamber and the concentrations were determined to reach a steady-
286 state equilibrium representative of the megalopolis atmosphere.

287 Following an entire day of VOCs injection, nitrogen monoxide was introduced when the lights
288 were turned on, simulating the tropospheric sunlight irradiation. Seed of ammonium sulfate
289 particles were next injected and formed contact surfaces for the condensation of oxidized
290 products. This resulted in the formation of Secondary Organic Aerosols (SOA), a complex and
291 reactive molecule, produced *via* the oxidation over several generations of a parent organic
292 molecule. These particles were produced from the nebulization of an ammonium sulfate
293 solution ($10^{-4}/10^{-3}\text{Mol.l}^{-1}$) through an atomizer. To be as representative as possible of a
294 Beijing-like atmosphere, soot particles were induced using a generator (mini-CAST Series
295 5200) producing soot particles by using a well-defined flame, based on the combustion of
296 propane. These particles were stocked into a reservoir and injected daily into the CESAM
297 chamber. Finally, to complete the simulation protocol, mineral dust particles, simulating a
298 desert storm *via* a mineral dust plume, were injected daily into the smog chamber. These
299 particles were produced through a shaking process from a Gobi Desert sample. Exposed mice
300 (EX) atmosphere was fed with a continuous flow coming from the CESAM smog chamber,
301 whereas the non-exposed mice (NE) were in a filtered clean air atmosphere. The atmospheric
302 environment to which mice were exposed was monitored by several instruments (NO_x
303 analyzer coupled with a NO₂ analyzer, O₃ analyzer, SO₂ analyzer, Fourier transform infrared
304 spectroscopy (FTIR), proton Transfer reaction Time of Flight mass spectrometry (PTR-TOF-
305 MS), gas chromatography Flame Ionisation Detector (GC-FID), SMPS for the particulate
306 matter, light-scattering aerosol, and an Aerosol Chemical Speciation Monitor (ACSM) for
307 aerosol specification). Regarding the “classical” indicators of air quality, in our study, we
308 observed these following maximum average concentrations; for nitrogen dioxide (NO₂) 35.64
309 ± 14.08 ppb for exposed mice versus 0.98 ± 0.43 ppb for the non-exposed one, for sulfur

310 dioxide (SO₂) 25.82 ± 10.72 ppb for exposed mice versus 0.98 ± 0.43 ppb for the non-exposed
311 ones. Finally for the concentration of particles we observed a maximum average concentration
312 of 216.74 ± 116.64 µg/m³ for exposed mice and 0.60 ± 1.33 µg/m³ for the non-exposed. In this
313 study, the mice were exposed for 7 days,, then the lungs were collected to analyze the effects
314 of urban pollution on the alveolar stem cell and niche properties.

315

316

317

318

319

320

321

322

323

324

325

326

327

328

329

330

331

332

333

334

335

336

337

338 **Urban atmosphere alters alveolar mesenchymal niche properties**

339 The effect of air pollution on the alveolar mesenchymal cells has yet to be determined. As
340 such, we first assessed the niche properties of lung fibroblasts isolated from mice exposed
341 (referred to herein as F-EX) or not (F-NE) to the urban atmosphere (Figure 2A). After 7 days
342 of air pollution exposure, the isolated fibroblasts were cultured and passaged to perform a
343 cumulative population doubling level (PDL). F-EX presented a lower PDL compared to F-NE
344 after the third passage ($p \leq 0.05$, $n=6$ for each group, Figure 2B). We next used an organoid 3D
345 culture approach to investigate their supportive niche capacities. F-EX and F-NE were mixed
346 with lung epithelial cells, EpCAM+, isolated from unexposed naïve mice lungs. Organoids
347 were imaged at day 14 and 21 (Figure 2C and D), the size and number of organoids per well
348 were quantified (Figure 2E and F). The number of organoids formed with F-EX was lower
349 compared to F-NE at day 14 and 21 (respectively 6.80 ± 0.83 for F-EX vs 18.90 ± 2.01 for F-NE
350 and 10.85 ± 1.87 vs 25.09 ± 1.97 ; $n=13$ for F-NE and $n=10$ for F-EX; $p < 0.0001$). Moreover, the
351 organoid number significantly increased between day 14 and day 21 (25.01 ± 1.91 at day 21 vs
352 18.90 ± 2 at day 21; $p=0.0246$) for F-NE but no difference was noted for F-EX. The same
353 pattern was observed for the size quantification ($76.01 \pm 1.68 \mu\text{m}$ for F-EX vs $85.32 \pm 1.53 \mu\text{m}$
354 for F-NE at day 14 and $83.06 \pm 1.65 \mu\text{m}$ vs $93.74 \pm 1.60 \mu\text{m}$ at day 21; $p < 0.0001$). Here, we
355 demonstrated a deterioration of fibroblast proliferation, assessed by the PDL assay, associated
356 with failure to form organoids, suggesting an alteration of alveolar mesenchymal niche
357 properties following urban atmosphere exposure.

358

359

360

361

362

363

364

365

366

367

368

369 **Urban atmosphere induced a lipofibroblast to myofibroblast switch associated with a**
370 **fibrotic phenotype**

371 To further understand by which mechanism urban atmosphere affects the mesenchymal cell
372 properties, we performed a microarray analysis on F-EX (n=4) and F-NE (n=3), at passage 3.
373 Among the 504 genes significantly modulated by urban atmosphere exposure, 295 were
374 downregulated and 209 upregulated (Figure 3A). Pathways analysis results highlighted a
375 downregulation of the expression gene associated with the regulation of WNT and FGF
376 signaling, pluripotent stem cell differentiation, and adipogenesis pathways. Conversely, genes
377 associated with pulmonary fibrosis, asthma, PI3K and HIF-1 signaling pathways were
378 upregulated (Figure 3B). Because of the importance of lipofibroblasts in stem cell niche
379 properties, we queried the LIF-associated pathway and highlighted the main differentially
380 expressed genes in adipogenesis and fibrosis (Figure 3). Adipogenesis associated genes:
381 *SFRP1*, *FGF2* or *FGF10* were downregulated in F-EX compared to F-NE. In contrast,
382 fibrosis associated genes: *SERPINI*, *PDGF α* or *ACTA2* were upregulated in F-EX. (Figure
383 3C). These results were confirmed by RT-qPCR analysis on whole lung tissues. *ADRP* and
384 *COL1A1* expression (LIF markers) significantly decreased in EX lung mice compared to NE
385 (Respectively 0.010 ± 0.0006 vs 0.016 ± 0.0014 ; $p=0.0026$ and 0.555 ± 0.1376 vs 1.115 ± 0.1353 ;
386 $p=0.0158$; $n=6$; Figure 3D-E). Conversely, *ACTA2* (myofibroblast marker) increased in EX
387 lung mice compared to NE (0.071 ± 0.006 vs 0.051 ± 0.005 , $p=0.0412$; $n=6$; Figure 3F).
388 Moreover, *FGF10* downregulation in NE was also confirmed (0.0026 ± 0.0005 vs
389 0.0073 ± 0.0007 ; $p=0.0004$; $n=6$, Figure 3G).

390 Following these results, we confirmed the fibrosis pattern by measuring collagen deposition
391 with Sirius red (Figure 3H and I). Results showed a significant increase of the Sirius red
392 staining in EX mice lungs compared to NE ($38.60 \pm 4.4\%$ vs $23.31 \pm 1.4\%$; $n=6$; $p=0.0152$;
393 Figure 3J). Given the ability of lipofibroblasts to differentiate into myofibroblasts in lung
394 fibrosis, we tested whether urban atmosphere increased myofibroblast content in the whole
395 lung. Immunostaining for ADRP (lipofibroblasts maker) and α -SMA (myofibroblast marker)
396 was performed (Figure 3K and 3L). The quantification of the total positive cells demonstrated
397 a decrease of ADRP (10.91 ± 2.07 in EX vs 53.03 ± 3.197 in NE; $n=12$; $p=0.0012$; Figure 3M)
398 and an increase of α -SMA (46.60 ± 2.652 vs 19.52 ± 1.203 ; $n=12$; $p<0.0001$; Figure 3N) in EX
399 mice lungs vs NE. Thus, these results suggested that urban atmosphere may induce a
400 lipofibroblast to myofibroblast switch associated with a fibrotic phenotype.

401

402

403 **Urban atmosphere directly and indirectly altered AT2 to AT1 transition**

404 We next investigated whether the mesenchymal niche alterations observed after exposure to
405 air pollution were associated with alveolar epithelial dysfunction. We first sought to measure
406 the impact of pollution on alveolar epithelial proliferation by staining for SFTPC (AT2 cells)
407 and KI67 in NE versus EX mice lungs (Figure 4A and B). Our results demonstrated a
408 decrease of the total AT2 cell number after urban atmosphere exposure ($9.944\pm 0.4\%$ in EX vs
409 $12.47\pm 0.6\%$ in NE, $n=8$; $p= 0.0143$; Figure 4C). However, we observed an increase in the
410 proliferative abilities of AT2 cells as shown by SFTPC+/KI67+ cells after exposure
411 ($0.181\pm 0.06\%$ in EX vs $0.023\pm 0.01\%$ in NE; $n=8$; $p=0.0208$; Figure 4D). It has been recently
412 demonstrated that lung fibrosis is associated with the emergence of a transitional cell state
413 characterized by failure of AT2 cells to fully transition to AT1 cells³⁴. These cells are named
414 ‘alveolar differentiation intermediate’ (ADI) and are SFTPC negative (SFTPC⁻), Keratin-8-
415 positive (KRT8⁺) and Claudin-4-positive (CLDN4⁺)³⁵. Given that we observed a fibrotic-like
416 phenotype in the exposed lungs, we investigated the presence of ADI cells (Figure 4E and F).
417 We observed a significant increase of KRT8+ cells after urban pollution exposure
418 ($3.935\pm 0.4\%$ in EX vs $1.354\pm 0.12\%$ in NE; $n=8$, $p= 0.0002$; Figure 4G). In addition, our
419 results showed that SFTPC⁻/KRT8⁺/CLDN4⁺ cells, ADI cells, were in significantly greater
420 number following air pollution exposure ($6.445\pm 1.65\%$ in EX vs $2.011\pm 0.55\%$ in NE; $n=6$;
421 $p= 0.0296$; Figure 4H). These results suggest a possible alteration of the alveolar epithelial
422 stem cell properties due to an effect from the surrounding mesenchyme, and/or due to a direct
423 effect of pollution.

424 To assess the direct effect of pollution on alveolar epithelial cells, we performed an organoid
425 assay, this time by using EpCAM+ cells isolated from the lungs of mice exposed (E-EX) or
426 not (E-NE) to urban atmosphere, mixed with fibroblasts isolated from naive lungs (Figure 4I
427 and J). Results showed, as for F-EX, a significant decrease of the organoids number per well
428 at day 14 and 21 (respectively 5.111 ± 1.62 for E-EX vs 12.20 ± 2.5 for E-NE and 9.714 ± 1.61
429 for E-EX vs 16.57 ± 1.71 for E-NE; $n=10$; $p= 0.0131$, Figure 4K). If no difference was noted at
430 day 14, the organoids size was significantly reduced at day 21 for E-EX ($94.75\mu\text{m}\pm 3.12$ in E-
431 EX vs $105,6\mu\text{m}\pm 3.91$ in E-NE; $p=0.0431$, Figure 4L). Altogether, the results indicate that
432 urban pollution may have a negative impact on both mesenchymal and epithelial cells,
433 potentially disrupting the repair and regeneration process.

434

435

436 **Discussion**

437 Urban pollution is today a global scourge continually associated with pulmonary pathologies
438 ^{36–38}. However, the underlying molecular and cellular mechanisms remain unknown,
439 especially as it pertains to the injury caused by pollution and the repair and regeneration
440 process following exposure.

441 Previous studies, involving exposure to a single component of air pollution, such as PM 2.5
442 ^{39,40}, ozone ^{41,42}, SO₂ ^{43,44} or the VOCs ^{45,46}, were associated to lung damages in mice and
443 human ⁴⁷. The effect of these individual exposures on alveoli, and specifically AT2 cells, or
444 the surrounding mesenchymal niche are diverse, ranging from inflammation to acute damage
445 or emphysema ^{10,48,49}, rendering it difficult to determine the specific alveolar pathologic
446 consequences of urban pollution. However, none of these models mimic the complexity of
447 urban atmosphere, particularly because they did not consider the interactions between
448 pollutants in the air or in the lung. In this study, we developed a unique and original model
449 that allow us to simulate a multi-pollutant exposure that mimic high levels of air pollution,
450 notably a megalopolis atmosphere like Beijing, that closely resembles a real-life exposure and
451 reflect the lung alterations induced by urban pollution ³¹.

452 Lung mesenchymal cells play an important role in the establishment and maintenance of AT2
453 cells ^{18,19}. The aim of this study was to determine the impact of urban pollution on the alveoli
454 and whether the detrimental effects are mainly driven by defects in the AT2 cells regenerative
455 capacity, or the niche environment. In fact, some studies investigated the effect of air
456 pollution on either epithelial or mesenchymal cells separately ^{50–53}; but little is known about
457 its effect on both combined and/or the interactions between them. Using an organoid culture
458 model as a surrogate for alveolar regeneration, our results demonstrated that urban
459 atmosphere, potentially, directly affects the mesenchymal component of the alveoli thus
460 altering their niche properties. When associated with naive epithelial cells, fibroblasts isolated
461 from exposed mice lungs generate fewer and smaller alveolar organoids.

462 To identify the molecular processes associated with this phenotype, microarray analyses were
463 performed on exposed or non-exposed fibroblasts. Results reported many differentially
464 expressed genes associated with disturbed expression of important signaling pathways WNT
465 or FGF pathways. Prior studies described, that the expression of the WNT pathway, a major
466 pathway involved in homeostasis, development and stem cell functions is associated with lung
467 fibrosis, however the underlying mechanisms remain unclear ^{54–56}. Moreover, exposed
468 fibroblasts displayed less FGF10, a gene known to regulate the alveolar niche properties and

469 mesenchymal differentiation ⁵⁷⁻⁵⁹. Interestingly, the expression of genes associated with
470 fibrosis were increased while those associated with adipogenesis were decreased in F-EX and
471 whole lung of exposed mice. Thus, our data suggest that urban pollution may alter the niche
472 properties of the mesenchymal cells. This alteration is evident by the reduction of
473 lipofibroblast markers, known as a key player of the stem cell niche ^{11,38-39}, and an increase in
474 fibrosis markers. Sirius Red staining demonstrated an increase of collagen deposition in the
475 alveolar wall in exposed mice lungs. The decrease of ADRP and increase of α -SMA suggest a
476 lipofibroblast to myofibroblast switch, often associated with a pathologic phenotype ^{22-24,60,61}.
477 The reduced regenerative capacity assessed by organoid formation and the lipofibroblast to
478 myofibroblast switch are key factors contributing to lung fibrosis ^{62,63}.

479 In addition, we demonstrated that urban pollution induced an increase of intermediate SFTPC-
480 /KRT8+/CLDN4+ AT2 cells. Several studies described KRT8+ and CLDN4+ cells as
481 markers of a transitional AT2 cell state important during alveolar epithelial cell differentiation
482 ^{64,65}. However, the aberrant persistence of this state is associated with fibrosis consistent with
483 our findings ^{35,66}. Taken together these results demonstrated that urban pollution alters the
484 mesenchymal niche properties, induces fibrosis-like phenotype, and impairs alveolar
485 regeneration. Furthermore, using epithelial cells from lungs exposed to urban atmosphere
486 mixed with naive fibroblasts also altered organoid formation capacity, suggesting that urban
487 pollution have both a direct (independent from fibroblasts) and indirect effect on AT2 stem
488 cell regenerative capacity.

489 In conclusion, this study highlights the importance of using multiparameter pollution models
490 to first expose our mice to more realistic urban atmosphere and secondly to consider the
491 epithelial-mesenchymal interactions in the lung. The results depicted a deleterious effect of
492 urban pollution on alveolar stem cell niche properties leading to the appearance of a fibrotic
493 phenotype. Identifying the mechanisms underlying the effect of air pollution on lung
494 alveolarization and regeneration would help to develop new strategies allowing to repopulate
495 progenitor cells directly, or by acting through their mesenchymal niche once the alveolar
496 lesions are established. This will help reduce the burden of pollution-induced lung diseases.

497
498
499
500

501 **Limitations of study**

502 If the urban atmosphere exposure is an original approach to determine the impact of air
503 pollution on the lung, it remains difficult to determine which component of the atmosphere, or
504 which combination of components is the main drivers of the lung damage. In addition, a
505 longer exposure would also be interesting and more relevant to human real-life situations, to
506 better understand the long-term effect of urban pollution on lung. However, we were able to
507 highlight a clear effect of urban atmospheres, despite the short exposure time.

508

509

510

511

512

513

514

515

516

517

518

519

520

521

522

523

524

525

526

527

528

529

530 **References**

- 531 1. Salvador P, Pandolfi M, Tobías A, et al. Impact of mixing layer height variations on air pollutant
532 concentrations and health in a European urban area: Madrid (Spain), a case study. *Environ Sci*
533 *Pollut Res Int.* 2020;27(33):41702-41716.
- 534 2. Boudet C, Zmirou D, Déchenaux J. [Personal exposure to fine particles (PM 2.5) in the Grenoble
535 population: European EXPOLIS study]. *Rev Epidemiol Sante Publique.* 2000;48(4):341-350.
- 536 3. Seaton A. Particles in the air: the enigma of urban air pollution. *J R Soc Med.* 1996;89(11):604-
537 607.
- 538 4. Kumar P, Morawska L, Birmili W, et al. Ultrafine particles in cities. *Environ Int.* 2014;66:1-10.
- 539 5. Rager JE, Lichtveld K, Ebersviller S, et al. A toxicogenomic comparison of primary and
540 photochemically altered air pollutant mixtures. *Environ Health Perspect.* 2011;119(11):1583-
541 1589.
- 542 6. Sexton KG, Jeffries HE, Jang M, et al. Photochemical products in urban mixtures enhance
543 inflammatory responses in lung cells. *Inhal Toxicol.* 2004;16 Suppl 1:107-114.
- 544 7. Weitekamp CA, Stevens T, Stewart MJ, Bhawe P, Gilmour MI. Health effects from freshly
545 emitted versus oxidatively or photochemically aged air pollutants. *Sci Total Environ.*
546 2020;704:135772.
- 547 8. Terzano C, Di Stefano F, Conti V, Graziani E, Petroianni A. Air pollution ultrafine particles:
548 toxicity beyond the lung. *Eur Rev Med Pharmacol Sci.* 2010;14(10):809-821.
- 549 9. Ni L, Chuang CC, Zuo L. Fine particulate matter in acute exacerbation of COPD. *Front Physiol.*
550 2015;6:294.
- 551 10. de Barros Mendes Lopes T, Groth EE, Veras M, et al. Pre- and postnatal exposure of mice to
552 concentrated urban PM2.5 decreases the number of alveoli and leads to altered lung function
553 at an early stage of life. *Environ Pollut.* 2018;241:511-520.
- 554 11. Wiegman CH, Li F, Ryffel B, Togbe D, Chung KF. Oxidative Stress in Ozone-Induced Chronic Lung
555 Inflammation and Emphysema: A Facet of Chronic Obstructive Pulmonary Disease. *Front*
556 *Immunol.* 2020;11:1957.
- 557 12. Myatt TA, Vincent MS, Kobzik L, Naeher LP, MacIntosh DL, Suh H. Markers of inflammation in
558 alveolar cells exposed to fine particulate matter from prescribed fires and urban air. *J Occup*
559 *Environ Med.* 2011;53(10):1110-1114.
- 560 13. Orona NS, Astort F, Maglione GA, Saldiva PHN, Yakisich JS, Tasat DR. Direct and indirect air
561 particle cytotoxicity in human alveolar epithelial cells. *Toxicol In Vitro.* 2014;28(5):796-802.
- 562 14. Barkauskas CE, Cronce MJ, Rackley CR, et al. Type 2 alveolar cells are stem cells in adult lung. *J*
563 *Clin Invest.* 2013;123(7):3025-3036.
- 564 15. Wu A, Song H. Regulation of alveolar type 2 stem/progenitor cells in lung injury and
565 regeneration. *Acta Biochim Biophys Sin (Shanghai).* 2020;52(7):716-722.

- 566 16. Juul NH, Stockman CA, Desai TJ. Niche Cells and Signals that Regulate Lung Alveolar Stem Cells
567 In Vivo. *Cold Spring Harb Perspect Biol.* 2020;12(12):a035717.
- 568 17. Nasri A, Foisset F, Ahmed E, et al. Roles of Mesenchymal Cells in the Lung: From Lung
569 Development to Chronic Obstructive Pulmonary Disease. *Cells.* 2021;10(12):3467.
- 570 18. Taghizadeh S, Heiner M, Vazquez-Armendariz AI, et al. Characterization in mice of the resident
571 mesenchymal niche maintaining AT2 stem cell proliferation in homeostasis and disease. *Stem*
572 *Cells.* 2021;39(10):1382-1394.
- 573 19. Ma C, Liu Y, Ma Y, et al. Identification and characterization of pulmonary mesenchymal stem
574 cells derived from rat fetal lung tissue. *Tissue Cell.* 2021;73:101628.
- 575 20. Zepp JA, Zacharias WJ, Frank DB, et al. Distinct Mesenchymal Lineages and Niches Promote
576 Epithelial Self-Renewal and Myofibrogenesis in the Lung. *Cell.* 2017;170(6):1134-1148.e10.
- 577 21. Cassandras M, Wang C, Kathiriya J, et al. Gli1+ mesenchymal stromal cells form a pathological
578 niche to promote airway progenitor metaplasia in the fibrotic lung. *Nat Cell Biol.*
579 2020;22(11):1295-1306.
- 580 22. Zysman M, Baptista BR, Essari LA, et al. Targeting p16INK4a Promotes Lipofibroblasts and
581 Alveolar Regeneration after Early-Life Injury. *Am J Respir Crit Care Med.* 2020;202(8):1088-
582 1104.
- 583 23. Ushakumary MG, Riccetti M, Perl AKT. Resident interstitial lung fibroblasts and their role in
584 alveolar stem cell niche development, homeostasis, injury, and regeneration. *Stem Cells Transl*
585 *Med.* 2021;10(7):1021-1032.
- 586 24. El Agha E, Herold S, Al Alam D, et al. Fgf10-positive cells represent a progenitor cell population
587 during lung development and postnatally. *Development.* 2014;141(2):296-306.
- 588 25. Torday JS, Torres E, Rehan VK. The role of fibroblast transdifferentiation in lung epithelial cell
589 proliferation, differentiation, and repair in vitro. *Pediatr Pathol Mol Med.* 2003;22(3):189-207.
- 590 26. Katsura H, Sontake V, Tata A, et al. Human Lung Stem Cell-Based Alveolospheres Provide
591 Insights into SARS-CoV-2-Mediated Interferon Responses and Pneumocyte Dysfunction. *Cell*
592 *Stem Cell.* 2020;27(6):890-904.e8.
- 593 27. Abo KM, Ma L, Matte T, et al. Human iPSC-derived alveolar and airway epithelial cells can be
594 cultured at air-liquid interface and express SARS-CoV-2 host factors. *bioRxiv.* Published online
595 June 4, 2020:2020.06.03.132639.
- 596 28. Fujii M, Matano M, Toshimitsu K, et al. Human Intestinal Organoids Maintain Self-Renewal
597 Capacity and Cellular Diversity in Niche-Inspired Culture Condition. *Cell Stem Cell.*
598 2018;23(6):787-793.e6.
- 599 29. Lu T, Cao Y, Zhao P, Shen S, Xi Y. Organoid: a powerful tool to study lung regeneration and
600 disease. *Cell Regen.* 2021;10(1):21.
- 601 30. Murrow LM, Weber RJ, Gartner ZJ. Dissecting the stem cell niche with organoid models: an
602 engineering-based approach. *Development.* 2017;144(6):998-1007.

- 603 31. Guilloteau E, Coll P, Lu Z, et al. Murine in utero exposure to simulated complex urban air
604 pollution disturbs offspring gut maturation and microbiota during intestinal suckling-to-
605 weaning transition in a sex-dependent manner. *Part Fibre Toxicol.* 2022;19(1):41.
- 606 32. Chen J, Xu H, Aronow BJ, Jegga AG. Improved human disease candidate gene prioritization
607 using mouse phenotype. *BMC Bioinformatics.* 2007;8(1):392.
- 608 33. Coll P, Cazaunau M, Boczkowski J, et al. POLLURISK: AN INNOVATIVE EXPERIMENTAL PLATFORM
609 TO INVESTIGATE HEALTH IMPACTS OF AIR QUALITY. In: ; 2018:557-565.
- 610 34. Kobayashi Y, Tata A, Konkimalla A, et al. Persistence of a regeneration-associated, transitional
611 alveolar epithelial cell state in pulmonary fibrosis. *Nat Cell Biol.* 2020;22(8):934-946.
- 612 35. Strunz M, Simon LM, Ansari M, et al. Alveolar regeneration through a Krt8+ transitional stem
613 cell state that persists in human lung fibrosis. *Nat Commun.* 2020;11(1):3559.
- 614 36. Guarnieri M, Balmes JR. Outdoor air pollution and asthma. *Lancet.* 2014;383(9928):1581-1592.
- 615 37. Shamsollahi HR, Jahanbin B, Rafieian S, Yunesian M. Particulates induced lung inflammation
616 and its consequences in the development of restrictive and obstructive lung diseases: a
617 systematic review. *Environ Sci Pollut Res Int.* 2021;28(20):25035-25050.
- 618 38. D'Amato G, Cecchi L, D'Amato M, Liccardi G. Urban air pollution and climate change as
619 environmental risk factors of respiratory allergy: an update. *J Investig Allergol Clin Immunol.*
620 2010;20(2):95-102; quiz following 102.
- 621 39. Li J, Hu Y, Liu L, Wang Q, Zeng J, Chen C. PM2.5 exposure perturbs lung microbiome and its
622 metabolic profile in mice. *Sci Total Environ.* 2020;721:137432.
- 623 40. Li R, Zhou R, Zhang J. Function of PM2.5 in the pathogenesis of lung cancer and chronic airway
624 inflammatory diseases. *Oncol Lett.* 2018;15(5):7506-7514.
- 625 41. Hwang BF, Chen YH, Lin YT, Wu XT, Leo Lee Y. Relationship between exposure to fine
626 particulates and ozone and reduced lung function in children. *Environ Res.* 2015;137:382-390.
- 627 42. Sokolowska M, Quesniaux VFJ, Akdis CA, Chung KF, Ryffel B, Togbe D. Acute Respiratory Barrier
628 Disruption by Ozone Exposure in Mice. *Front Immunol.* 2019;10:2169.
- 629 43. Meng Z, Qin G, Zhang B, et al. Oxidative damage of sulfur dioxide inhalation on lungs and hearts
630 of mice. *Environ Res.* 2003;93(3):285-292.
- 631 44. Wigenstam E, Elfsmark L, Bucht A, Jonasson S. Inhaled sulfur dioxide causes pulmonary and
632 systemic inflammation leading to fibrotic respiratory disease in a rat model of chemical-induced
633 lung injury. *Toxicology.* 2016;368-369:28-36.
- 634 45. Wang F, Li C, Liu W, Jin Y, Guo L. Effects of subchronic exposure to low-dose volatile organic
635 compounds on lung inflammation in mice. *Environ Toxicol.* 2014;29(9):1089-1097.
- 636 46. Zhang JJ, Wei Y, Fang Z. Ozone Pollution: A Major Health Hazard Worldwide. *Front Immunol.*
637 2019;10:2518.

- 638 47. Churg A, Brauer M, del Carmen Avila-Casado M, Fortoul TI, Wright JL. Chronic exposure to high
639 levels of particulate air pollution and small airway remodeling. *Environ Health Perspect.*
640 2003;111(5):714-718.
- 641 48. Falcon-Rodriguez CI, Osornio-Vargas AR, Sada-Ovalle I, Segura-Medina P. Aeroparticles,
642 Composition, and Lung Diseases. *Front Immunol.* 2016;7:3.
- 643 49. Nishimura Y, Maeda M, Kumagai-Takei N, et al. Altered functions of alveolar macrophages and
644 NK cells involved in asbestos-related diseases. *Environ Health Prev Med.* 2013;18(3):198-204.
- 645 50. Cervellati F, Woodby B, Benedusi M, Ferrara F, Guiotto A, Valacchi G. Evaluation of oxidative
646 damage and Nrf2 activation by combined pollution exposure in lung epithelial cells. *Environ Sci*
647 *Pollut Res Int.* 2020;27(25):31841-31853.
- 648 51. Jia H, Liu Y, Guo D, He W, Zhao L, Xia S. PM2.5-induced pulmonary inflammation via activating
649 of the NLRP3/caspase-1 signaling pathway. *Environ Toxicol.* 2021;36(3):298-307.
- 650 52. Estrella B, Naumova EN, Cepeda M, Voortman T, Katsikis PD, Drexhage HA. Effects of Air
651 Pollution on Lung Innate Lymphoid Cells: Review of In Vitro and In Vivo Experimental Studies.
652 *Int J Environ Res Public Health.* 2019;16(13):E2347.
- 653 53. Gao Y, Huang X, Lin H, et al. Adipose mesenchymal stem cell-derived antioxidative extracellular
654 vesicles exhibit anti-oxidative stress and immunomodulatory effects under PM2.5 exposure.
655 *Toxicology.* 2021;447:152627.
- 656 54. Villar J, Zhang H, Slutsky AS. Lung Repair and Regeneration in ARDS: Role of PECAM1 and Wnt
657 Signaling. *Chest.* 2019;155(3):587-594.
- 658 55. Van Camp JK, Beckers S, Zegers D, Van Hul W. Wnt signaling and the control of human stem cell
659 fate. *Stem Cell Rev Rep.* 2014;10(2):207-229.
- 660 56. Burgy O, Königshoff M. The WNT signaling pathways in wound healing and fibrosis. *Matrix Biol.*
661 2018;68-69:67-80.
- 662 57. Volckaert T, De Langhe S. Lung epithelial stem cells and their niches: Fgf10 takes center stage.
663 *Fibrogenesis Tissue Repair.* 2014;7:8.
- 664 58. Yuan T, Volckaert T, Redente EF, et al. FGF10-FGFR2B Signaling Generates Basal Cells and Drives
665 Alveolar Epithelial Regeneration by Bronchial Epithelial Stem Cells after Lung Injury. *Stem Cell*
666 *Reports.* 2019;12(5):1041-1055.
- 667 59. Wu J, Chu X, Chen C, Bellusci S. Role of Fibroblast Growth Factor 10 in Mesenchymal Cell
668 Differentiation During Lung Development and Disease. *Front Genet.* 2018;9:545.
- 669 60. Sakurai R, Liu J, Wang Y, Torday JS, Rehan VK. Prevention of perinatal nicotine-induced bone
670 marrow mesenchymal stem cell myofibroblast differentiation by augmenting the lipofibroblast
671 phenotype. *Clin Sci (Lond).* 2018;132(21):2357-2368.
- 672 61. Lv YQ, Dhlamini Q, Chen C, Li X, Bellusci S, Zhang JS. FGF10 and Lipofibroblasts in Lung
673 Homeostasis and Disease: Insights Gained From the Adipocytes. *Front Cell Dev Biol.*
674 2021;9:645400.

675 62. Lingampally A, Jones MR, Bagari S, Chen C, Rivetti S, Bellusci S. Use of the Reversible Myogenic
676 to Lipogenic Transdifferentiation Switch for the Design of Pre-clinical Drug Screening in
677 Idiopathic Pulmonary Fibrosis. *Front Bioeng Biotechnol.* 2020;8:569865.

678 63. Kheirollahi V, Wasnick RM, Biasin V, et al. Metformin induces lipogenic differentiation in
679 myofibroblasts to reverse lung fibrosis. *Nat Commun.* 2019;10(1):2987.

680 64. Jiang P, Gil de Rubio R, Hrycaj SM, et al. Ineffectual Type 2-to-Type 1 Alveolar Epithelial Cell
681 Differentiation in Idiopathic Pulmonary Fibrosis: Persistence of the KRT8hi Transitional State.
682 *Am J Respir Crit Care Med.* 2020;201(11):1443-1447.

683 65. Liapustin VN, Gritsun TS, Lashkevich VA. [Characteristics of incorporation of carbohydrate
684 radioactivity into structural proteins of the tick-borne encephalitis virus]. *Mol Gen Mikrobiol*
685 *Virusol.* 1987;(3):24-26.

686 66. Xie T, Lynn H, Parks WC, et al. Abnormal respiratory progenitors in fibrotic lung injury. *Stem Cell*
687 *Res Ther.* 2022;13(1):64.

688

689

690

691

692

693

694

695

696

697

698

699

700

701

702

703

704

705

706 **Acknowledgments**

707 We thank Stephane Kerbat and Denis Mestivier (IMRB, Genomic platform, INSERM) and
708 l'Agence nationale de sécurité sanitaire de l'alimentation, de l'environnement et du travail
709 (ANSES) who supported the call of the project EST-2019-200.

710

711

712 **Author Contributions**

713 RB, BRB, PC, SL and LB designed the research studies, RB, BRB, GJ, MT, RY, PC and LB
714 conducted the experiments, RB, BRB, GJ, MT and RY acquired data, RB, BRB MT, AF, PC
715 and LB analyzed the data, RB, BRB, GJ, MT, AF, RY, ADV, MC, EP, AB, AG, JCMR, SB,
716 GD, JB, DAA, PC, SL and LB wrote edited and approved the final manuscript. No
717 honorarium or other form of payment was given to anyone to produce the manuscript.

718

719

720 **Declaration of Interests**

721 The authors have declared that no conflict of interest exists.

722

723

724

725

726

727

728

729

730

731

732

733

734

735

736

737

738

739

740 **Figure Legends**

741 **Figure 1. Atmospheric chamber generated urban pollution exposure.** (A) View of the
742 PolluRisk platform (Créteil, France) with the CESAM smog chamber in the background
743 topped with 3 Xenon lamps (1) simulating the sun's flux at the troposphere level. In left front,
744 we have the two mice exposure devices back-to-back (2), and at the front right the soot particle
745 reservoir (3). (B) A schematic view of the atmospheric simulation, to simulate realistic episode
746 of air pollution, various gaseous and particulate micro-pollutants (left section) are continuously
747 injected to the CESAM smog chamber, where photochemical steady-state equilibrium is
748 maintained for days, leading to hundreds of pollutants (gas and aerosols) representative of the
749 chemical composition of an urban complex atmospheric environment, as the one of Beijing. In
750 the right, mice are exposed (top) or not (bottom) to the simulated atmosphere and instruments
751 allow the control of quality and quantity of the pollutant.

752

753 **Figure 2: Urban atmosphere alters alveolar mesenchymal stem cell niche properties.** (A)
754 Schematic diagram showing the steps from sacrifice to data acquisition. (B) Populations
755 doubling levels of mouse lung primary fibroblasts exposed to a non-polluted atmosphere (F-
756 NE; control) or an urban atmosphere exposure (F-EX; pollution) *in vivo* (n=6). Representative
757 images of murine organoids formed by F-NE or F-EX at day 14 and 21 (red arrow: organoids;
758 Figure 2C and D). Number (E) and size (F) of organoids formed with fibroblasts control (F-
759 NE, n=13) or exposed to urban atmosphere (F-EX; n=10; co-cultured with non-exposed
760 EpCAM+) at day 14 (D14) and day 21 (D21). Results are shown as dot plot and mean \pm SEM;
761 *p = 0.05 , ****p< 0.0001 and ns = not significant.

762 **Figure 3: Urban atmosphere induced a lipofibroblasts to myofibroblasts switch**
763 **associated with an alveolar fibrotic process.** (A) Volcano plot of differentially expressed
764 genes identified between F-NE and F-EX. The blue dots denote down-regulated gene
765 expression, the green dots denote up-regulated expression, and the black denote the gene
766 expression without marked differences. (B) Representation of the top 3 significantly enriched
767 pathways obtained using ToppFun platform, presented as clustered bar charts. In blue, the
768 down-regulated pathways and in red the up-regulated. (C) A heatmap of adipogenesis and
769 fibrosis-related genes was generated from a subset extracted from the list of significantly
770 expressed genes. Columns represent sample, while rows represent specific genes of interest.
771 The Z-score depicts a measure of distance, in standard deviations, away from the mean. The
772 relative value for each gene is depicted by color intensity, with yellow indicating upregulated

773 and black indicating downregulated genes. RT-qPCR for *ADRP* (D), *COL1A1* (E), *ACTA2*
774 (F) and *FGF10* (G) performed on fibroblast from mice lung NE or EX to air pollution (n=6).
775 Representative red Sirius staining on NE (H) and EX (I) lungs mice and quantification of the
776 red Sirius positive area by Halo software (n=6; J). Representative immunofluorescence of
777 lipofibroblasts (*ADRP*, in green) and myofibroblasts (α -SMA, in red) in NE (K) and EX (L)
778 lungs mice. Quantification of the total positive cells in percent for *ADRP* (M) and α -SMA (N)
779 excluding large airways and vessels (n=12 for each group). Results are shown as dot plot and
780 mean \pm SEM; *p = 0.05, **p = 0.01, ***p = 0.001, ****p<0.001.

781 **Figure 4: Urban atmosphere directly and indirectly altered AT2 to AT1 transition**

782 Representative immunofluorescence of AT2 (SFTPC, in green) and KI67 (red) of non-
783 exposed (A) and exposed (B) lungs mice. Quantification of SFTPC total positive cells (C)
784 and SFTPC/KI67 total positive cells (D) in percent (n=8 for each group). Representative
785 immunofluorescence for AT2 (SFTPC, in white) and ADI (KRT8, in red; CLDN4, in green)
786 of NE (E) and EX (F) lungs mice. Quantification of KRT8 total positive cells (G; n=8) and
787 SFTPC negative/KRT8-CLDN4 positive cells (H; n=6) in percent. Representative images of
788 murine organoids formed by EpCAM, co-cultured with non-exposed lung fibroblasts, from
789 non-exposed (E-NE) or exposed (E-EX) lungs mice at day 14 (I) and 21 (J) (red arrow:
790 organoids). Number (K; n=12) and size (L) of organoids formed by E-NE or E-EX at day 14
791 (D14) and 21 (D21). Results are shown as dot plot and mean \pm SEM; *p = 0.05, ***p = 0.001
792 and ns = not significant.

793

Figure 1: Atmospheric chamber generated urban pollution exposure

A



B

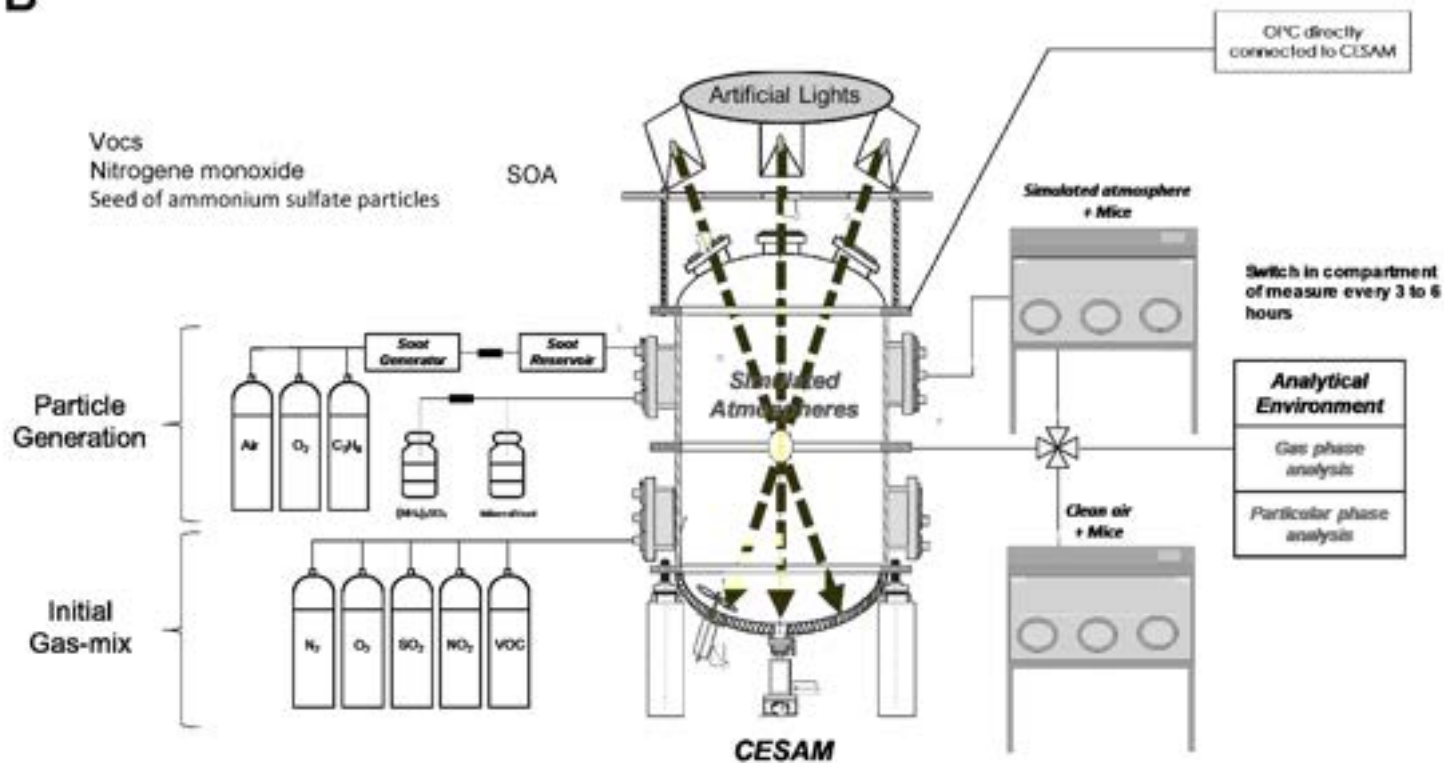


Figure 2 : Urban atmosphere alters alveolar mesenchymal stem cell niche properties

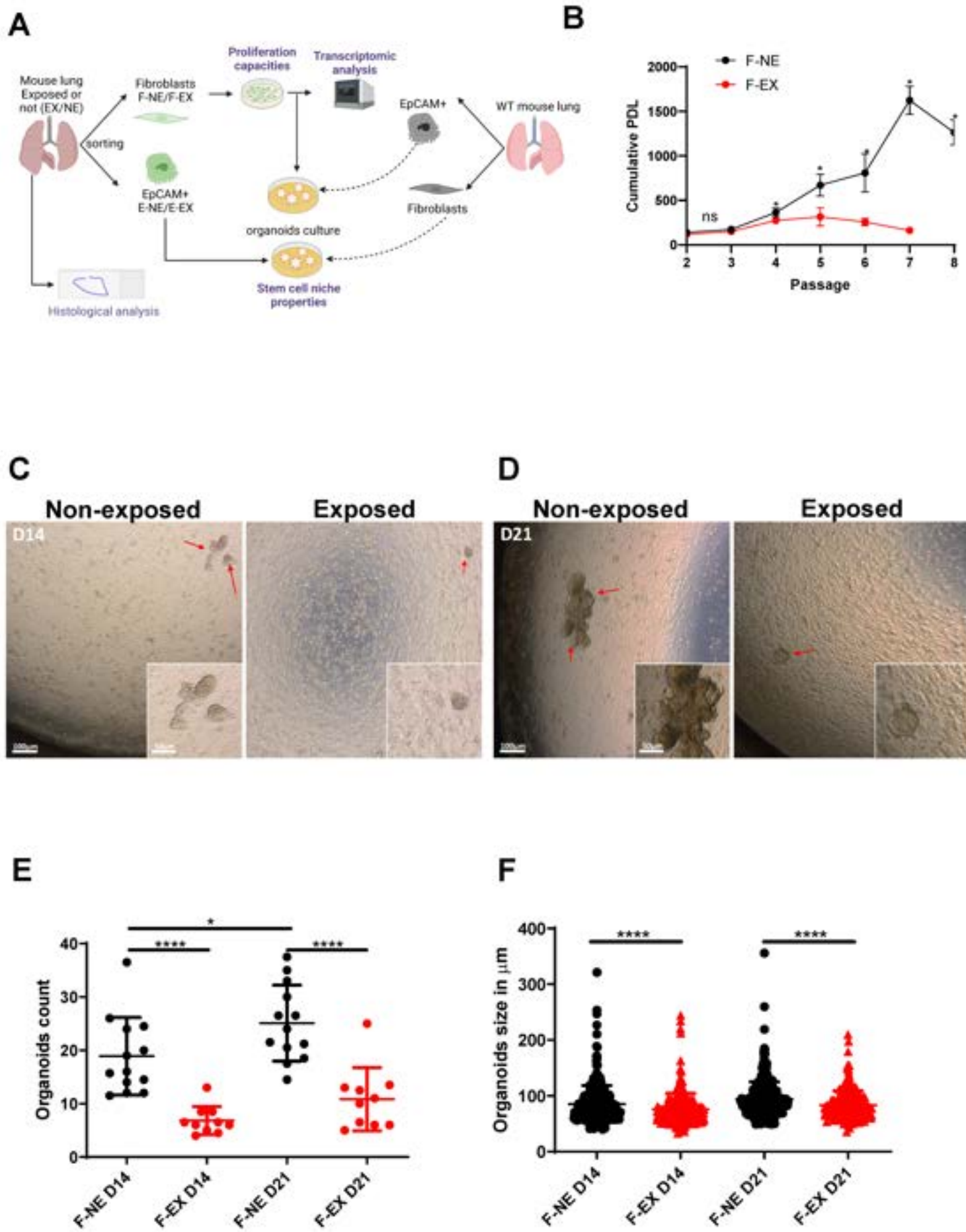


Figure 3: Urban atmosphere induced a lipofibroblasts to myofibroblasts switch associated with an alveolar fibrotic process

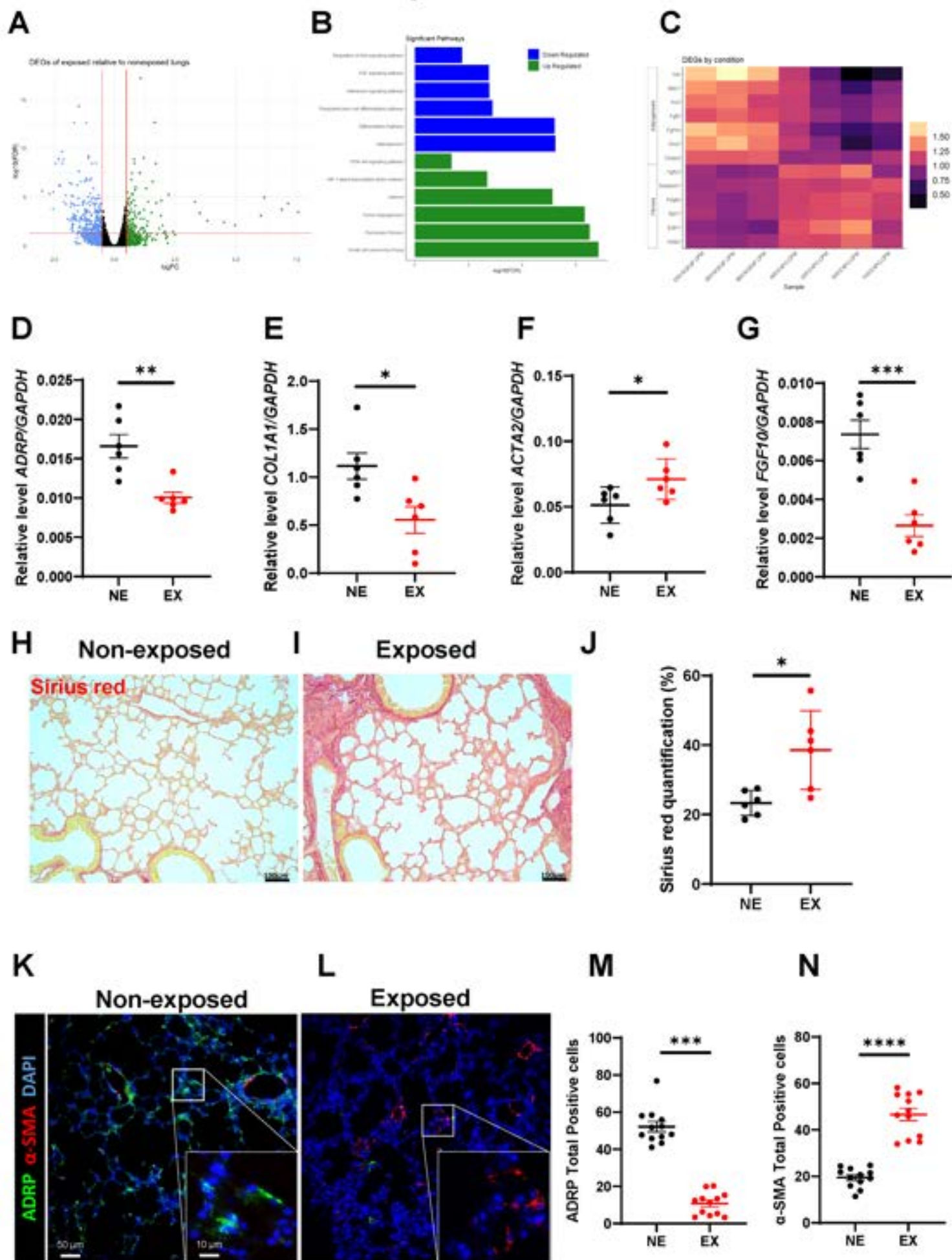
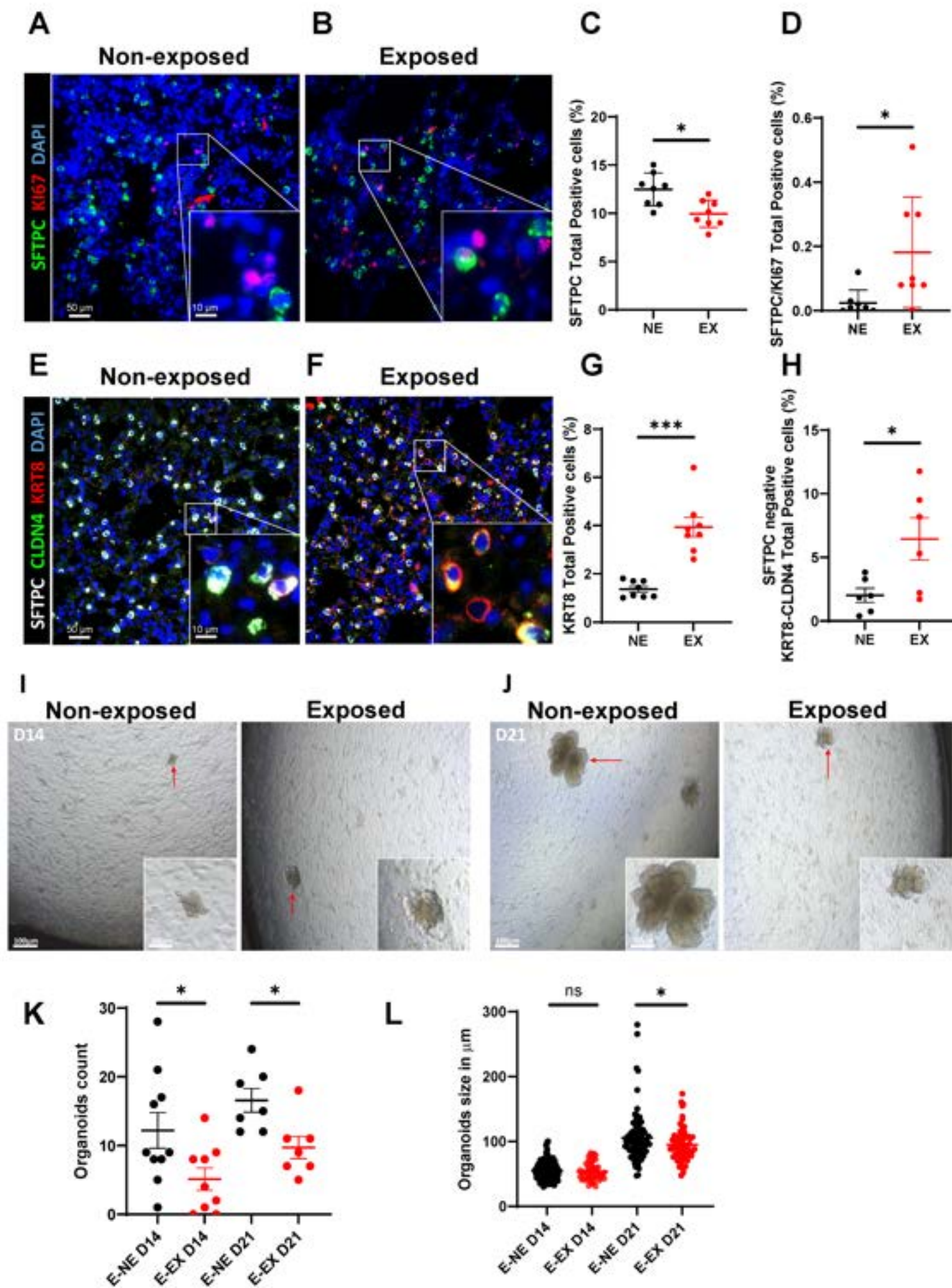
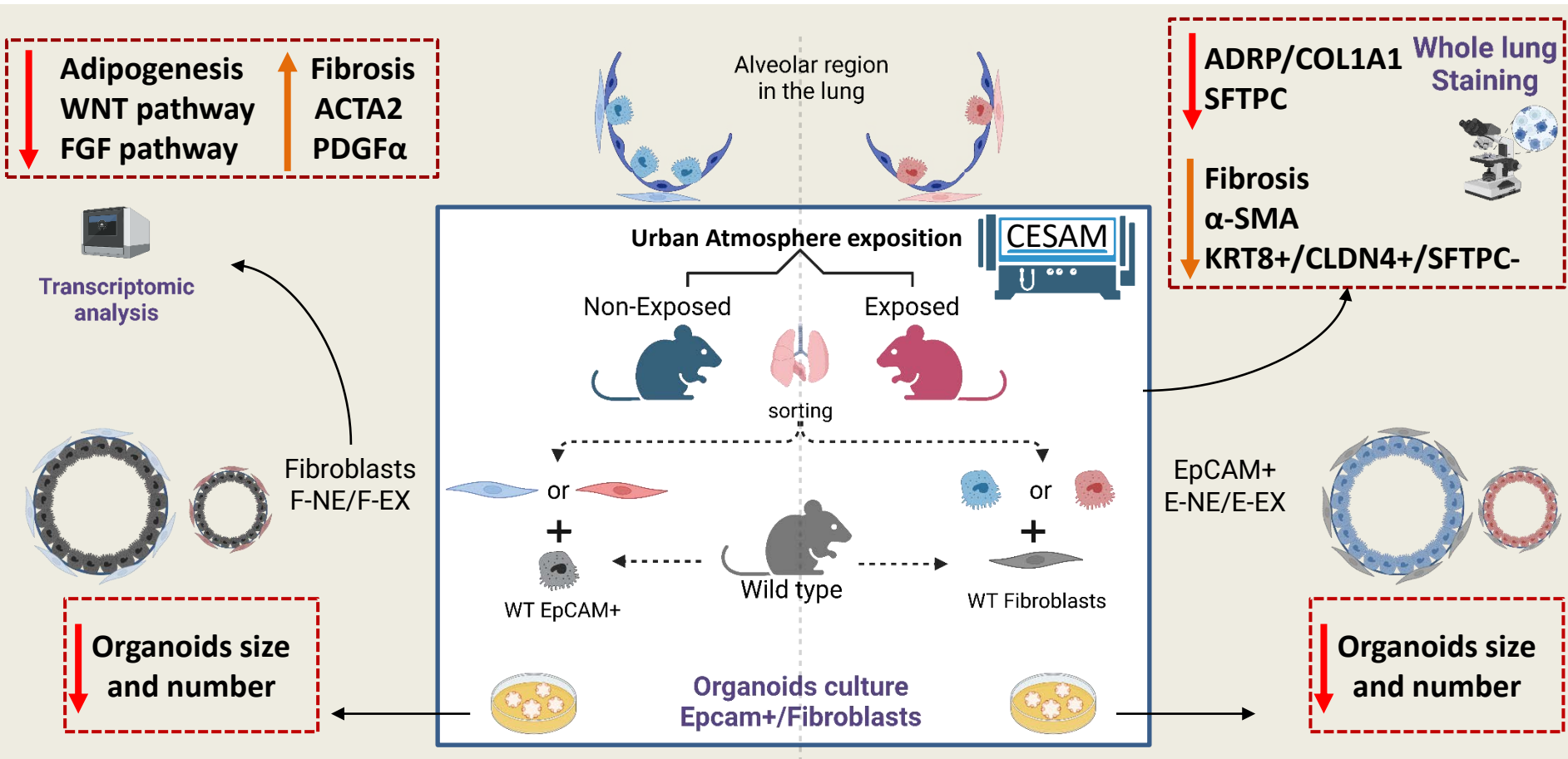


Figure 4: Urban atmosphere directly and indirectly altered AT2 to AT1 transition



Urban atmosphere alters stem cell niche properties



Exposure to Urban pollution impairs the regenerative capacity of AT2 cells and the ability of alveolar fibroblasts to act as a supportive niche